Driving Force and Isotope Dependence of the Kinetics of Proton-Coupled Electron Transfer in Oxoruthenium(IV) Polypyridyl Complexes

Brian T. Farrer and H. Holden Thorp*

Department of Chemistry, University of North Carolina at Chapel Hill, Chapel Hill, North Carolina 27599-3290

Received February 24, 1999

The kinetics of the comproportionation reaction of $Ru(tpy)(bpy)O^{2+}$ and $Ru(tpy)(bpy)OH_2^{2+}$ to produce $Ru(tpy)(bpy)OH^{2+}$ were evaluated in a series of complexes that were substituted on the 4′ position of the tpy ligand or the 4 and 4′ positions of the bpy ligand (tpy = 2,2′:6′,2″-terpyridine, bpy = 2,2′-bipyridine). These substitutions did not change the steric or coordination environments about the Ru−O linkage but did modulate the driving force ($-\Delta G°$) for comproportionation over a range of ∼8 kJ/mol. The comproportionation reaction, which involves a net hydrogen atom transfer between the metal complexes, showed a linear dependence of its rate constant on the driving force across the range studied, with a slope of 0.66 ± 0.06 for H_2O and 0.64 ± 0.05 for D_2O. Thus, the slopes were in reasonably good agreement with the value of 0.5 predicted by Marcus theory and, as also expected, showed no effect of the driving force on the isotope effect. The isotope effect for the $Ru(tpy)(bpy)O^{2+}$ complex (11.5) was significantly lower than that for $Ru(bpy)_2(py)O^{2+}$ (16.1) at the same driving force. The $Ru(bpy)_2(py)O^{2+}$ complex is more sterically crowded at the oxo ligand, so the likely origin of the isotope effect is the distance of transfer for the proton in the reaction.

Biological systems exploit proton-coupled electron transfer (PCET) to increase the rate of electron transfer, stabilize charge separation, effect multielectron substrate oxidation,[1,2] and generate proton gradients.[3] Photosystem II uses PCET to facilitate electron transfer in the cascade of events that ultimately leads to water oxidation and production of ATP.[4,5] In respiration, cytochrome *c* oxidase uses PCET to reduce oxygen and to generate the proton gradient necessary for energy storage.[6−8] Model studies have shown that electron transfer can be facilitated when crossing hydrogen-bonded interfaces if proton motion is coupled to the electron movement.[9−11]

Large isotope effects due to proton tunneling often accompany PCET and have been observed in enzymatic systems[12,13] and synthetic systems at low temperature.[14] Although large isotope effects due to tunneling are not generally observed at high temperatures in small molecule systems, abnormally high isotope effects have been observed at room temperature for polypyridyl complexes of oxoruthenium(IV) that involve proton and electron transfer to form hydroxoruthenium(III) and aquaruthenium(II) complexes.[15−18] In particular, the comproportionation reaction between $Ru(bpy)_2(py)O^{2+}$ and $Ru(bpy)_2(py)OH_2^{2+}$ is a PCET reaction that exhibits an isotope effect of 16.1 (bpy = 2,2′-bipyridine):[16]

$$Ru(bpy)_2(py)OH_2^{2+} + Ru(bpy)_2(py)O^{2+} \rightleftharpoons 2Ru(bpy)_2(py)OH^{2+} \quad (1)$$

These isotope effects have been attributed to the coupling between the electron transfer and proton tunneling from donor to acceptor. These systems offer a unique opportunity to evaluate the molecular factors leading to the large isotope effects in PCET at room temperature, using conventional stopped-flow kinetics.

The added complexity in predicting the rate of PCET is a result of coupling between proton and electron transfer; additional problems arise when proton tunneling and solvent dipole coupling are considered. Cukier has developed a theoretical foundation for the prediciton of PCET rates[19−21] and has applied it to the model system developed by Nocera where a metal donor is hydrogen bonded to a dinitrobenzene through a hydrogen-bonded interface.[9−11] The isotope effect dependence on the driving force ($-\Delta G°$) in hydride-transfer reactions between

(1) Meyer, T. J. *J. Electrochem. Soc.* **1984**, *131*, 221C.
(2) Pecoraro, V. L.; Baldwin, M. J.; Caudle, M. T.; Hsieh, W. Y.; Law, N. A. *Pure Appl. Chem.* **1998**, *70*, 925−929.
(3) Mitchell, P. *Science* **1979**, *206*, 1148−1159.
(4) Babcock, G. T.; Barry, B. A.; Debus, R. J.; Hoganson, C. W.; Atamian, M.; McIntosh, L.; Sithole, I.; Yocum, C. F. *Biochemistry* **1989**, *28*, 9557−9565.
(5) Paddock, M. L.; McPherson, P. H.; Feher, G.; Okamura, M. Y. *Proc. Natl. Acad. Sci. U.S.A.* **1990**, *87*, 6803−6807.
(6) Malmstrom, B. G. *Chem. Rev.* **1990**, *90*, 1247−1260.
(7) Malmstrom, B. G. *Acc. Chem. Res.* **1993**, *26*, 332−338.
(8) Chan, S. I.; Li, P. M. *Biochemistry* **1990**, *29*, 1−12.
(9) Kirby, J. P.; Roberts, J. A.; Nocera, D. G. *J. Am. Chem. Soc.* **1997**, *119*, 9230−9236.
(10) Roberts, J. A.; Kirby, J. P.; Nocera, D. G. *J. Am. Chem. Soc.* **1995**, *117*, 8051−8052.
(11) Turro, C.; Chang, C. K.; Leroi, G. E.; Cukier, R. I.; Nocera, D. G. *J. Am. Chem. Soc.* **1992**, *114*, 4013−4015.
(12) Kohen, A.; Klinman, J. P. *Acc. Chem. Res.* **1998**, *31*, 397−404.
(13) Bahnson, B. J.; Klinman, J. P. *Methods Enzymol.* **1995**, *249*, 373−397.
(14) Aratono, Y.; Matumoto, T.; Takayanagi, T.; Kumada, T.; Komaguchi, K.; Miyazaki, T. *J. Phys. Chem.* **1998**, *102*, 1501−1506.
(15) Binstead, R. A.; Moyer, B. A.; Samuels, G. J.; Meyer, T. J. *J. Am. Chem. Soc.* **1981**, *103*, 2897−2899.
(16) Binstead, R. A.; Meyer, T. J. *J. Am. Chem. Soc.* **1987**, *109*, 3287−3297.
(17) Thompson, M. S.; Meyer, T. J. *J. Am. Chem. Soc.* **1982**, *104*, 4106−4115.
(18) Roecker, L.; Meyer, T. J. *J. Am. Chem. Soc.* **1987**, *109*, 746−754.
(19) Cukier, R. I. *J. Phys. Chem.* **1994**, *98*, 2378−2381.
(20) Cukier, R. I. *J. Phys. Chem.* **1995**, *99*, 16101−16115.
(21) Cukier, R. I. *J. Phys. Chem.* **1996**, *100*, 15428−15443.

10.1021/ic9902323 CCC: $18.00
Published on Web 04/24/1999

NADH molecules, where tunneling is significant, has been investigated by Kreevoy.[22−24]

The effects of the driving force on electron transfer can be described by the Marcus equation:[25]

$$\Delta G^{\ddagger} = w^{r} + [\lambda/4 + \Delta G^{\circ}/2 + (\Delta G^{\circ})^{2}/4\lambda] \qquad (2)$$

where $\Delta G^{\ddagger}$ is the activation energy for electron transfer, w^{r} is the work required to bring the reactants together, and λ is the reorganizational energy for the reaction. Since PCET involves in part a single electron transfer, eq 2 might be expected to govern the driving force dependence of the reaction. When $\Delta G^{\circ} \ll \lambda$, the rate of the reactions described by eq 2 shows a linear dependence on the driving force with a slope of $^{1}/_{2}$; the range of driving forces that give this linear dependence is known as the normal region. For proton transfer, kinetic isotope effects are manifested in the equation as changes in λ,[26] so if Marcus theory also describes PCET in the normal region, a dependence of the isotope effect on the driving force would not be expected.

In this paper, the effect of the driving force on the rate and isotope effect of the comproportionation between complexes based on $Ru(tpy)(bpy)OH_2^{2+}$ and $Ru(tpy)(bpy)O^{2+}$ is discussed (tpy = 2,2′,2″-terpyridine).[27] These complexes offer advantages over $Ru(bpy)_2(py)O^{2+}$ in terms of faster absolute rates and greater ease of synthesizing a homologous series of electronically differentiated redox partners. The dependence of the rate constant on the driving force is successfully explained by Marcus theory in the normal region, and the isotope effect does not change significantly in the range of driving forces studied. The driving forces are relatively small (6−14 kJ/mol) compared to λ, which for simple electron transfer is generally >150 kJ/mol[25] and as much as 400 kJ/mol for hydride transfer in organic molecules.[28] A comparison of the $Ru(tpy)(bpy)O^{2+}$ and $Ru(bpy)_2(py)O^{2+}$ systems shows that the isotope effect increases with the steric bulk around the oxo/aqua ligand. Thus, the distance that the proton is transferred appears to be the primary determinant in the large isotope effect.

Experimental Section

Materials. 2,2′:6′,2″-terpyridine (tpy), 2,2′-dipyridyl (bpy), 4,4′-Me_2−bpy, $RuCl_3 \cdot xH_2O$, and D_2O (99.9 atom %) were purchased from Aldrich Chemical Co. 4′-Cl-tpy and 4′-EtO-tpy were prepared as demonstrated by Constable et al.[29] The 4,4′-Cl_2-bpy ligand was prepared by the method published by Cook et al.[30] The $[Ru(4'\text{-X-tpy})(4,4'\text{-}Y_2\text{-bpy})O](ClO_4)_2$ complexes were prepared analogously to the synthesis of $[Ru(tpy)(bpy)O](ClO_4)_2$,[27] except Cl_2 instead of Br_2 was used as the oxidant in the final step.[31] Complete details of the preparation of the metal complexes will be published elsewhere.[32] Na_2HPO_4 and NaH_2PO_4 were purchased from Mallinckrodt and used without further purification. House distilled water was further purified by passage through a Millipore Milli-Q water purification system. Glassy carbon working electrodes were purchased from Bioanalytical Systems (BAS). Vitreous carbon working electrodes were purchased from The Electrosynthesis Co. Ag/AgCl reference electrodes were purchased from Cypress Systems. Buffer solutions (50 mM phosphate) were made by dissolving 0.165 g of $NaH_2PO_4 \cdot H_2O$ and 0.365 g of $Na_2HPO_4 \cdot 7H_2O$ in 100 mL of H_2O and titrating with the appropriate 50 mM sodium phosphate solution to acquire the desired pH. To ensure that the pH/D in the buffer solutions were similar, the pH of a 1:1 H_2O/D_2O solution was read using a Corning pH meter 240. Recorded pHs are the pH read at the 1:1 ratio. The read pH, however, did not seem to vary with the D_2O content.

Measurements. Stopped-flow experiments were carried out at 298 ± 1 K on an OLIS-RSM stopped-flow apparatus. Scans were taken at the rate of 1000 scans/s, obtaining data from 350 to 550 nm for 1−5 s. Solutions of the metal−oxo complexes were prepared by dissolving a small amount of RuO^{2+} solid in 50 mM sodium phosphate buffer (pH 7.8). Half of this solution was held at a potential of +0.85 V (vs Ag/AgCl, Pt wire counter, vitreous carbon working) to ensure the absence of lower oxidation state Ru. The remaining half was reduced to $RuOH_2^{2+}$ via bulk electrolysis by holding at a potential of 0.0 V (vs Ag/AgCl, Pt wire counter, vitreous carbon working) to ensure absence of higher oxidation state complexes. Both solutions were diluted using buffer to obtain final concentrations. The solutions were then frozen in liquid nitrogen until just prior to use to preserve the integrity of the oxidation state. Freezing the solutions is more important for the RuO^{2+} because it is less stable than $RuOH_2^{2+}$.

Cross reactions between $Ru(tpy)(4,4'\text{-}Cl_2\text{-bpy})OH_2^{2+}$ and $Ru(tpy)(4,4'\text{-}Me_2\text{-bpy})O^{2+}$ were carried out similarly. The condition $[Ru(tpy)(4,4'\text{-}Me_2\text{-bpy})O^{2+}] = [Ru(tpy)(4,4'\text{-}Cl_2\text{-bpy})OH_2^{2+}]$ was met by determining the concentration of both compounds in the $RuOH_2^{2+}$ state, using the extinction coefficient of the peak near 480 nm and adjusting the concentration appropriately before performing bulk electrolysis on the Me_2-bpy derivative.

Data Analysis. The kinetic data were fit using SPECFIT,[33] which is a global analysis algorithm, employing singular value decomposition factor analysis.[34] The data were fit to the mechanism: $RuO^{2+} + RuOH_2^{2+} \rightleftharpoons 2RuOH^{2+}$. The initial concentrations of RuO^{2+} and $RuOH_2^{2+}$ were found using the $t = 0$ s scan at the maximum absorbance around 480 nm. If $[RuO^{2+}] = [RuOH_2^{2+}]$ and $[RuOH^{2+}] = 0$ at $t = 0$, then the concentration of $RuOH_2^{2+}$ can be determined. $[RuOH_2^{2+}] = A_{max}\,[b/(\epsilon_{II} + \epsilon_{IV})]$, where A_{max} is the maximum absorbance around 480 nm (the precise λ_{max} in this region was slightly different across the series of complexes), b is the path length of the cell (1.8 cm), and ϵ_{II} and ϵ_{IV} are the extinction coefficients for the $RuOH_2^{2+}$ and RuO^{2+}, respectively.

Electrochemistry. Cyclic voltammetry was carried out on a PAR model 273A potentiostat scanning from 100 to 900 mV at 20 mV/s using a glassy carbon working electrode, an Ag/AgCl reference, and Pt wire counter. Solutions of $RuOH_2^{2+}$ were made by dissolving a small amount of $RuOH_2^{2+}$ in 50 mM sodium phosphate buffer of pH = 7.8. The concentration of ruthenium was determined using the extinction coefficient at maximum of the MLCT band at around 480 nm. Square-wave voltammetry was carried out on a PAR model 273A potentiostat, scanning from 100 to 900 mV using a glassy carbon working electrode Ag/AgCl reference, and Pt wire counter. Pulse frequency was usually 1 Hz but was varied between 0.5 and 64 Hz in certain experiments. Pulse height was typically 25 mV but was varied between 2 and 50 mV in some experiments. Step height was typically 1 mV but was varied between 1 and 16 mV in certain experiments. Samples for square-wave voltammetry were prepared by initially dissolving a small amount of ruthenium in 2× concentrated sodium phosphate buffer (for 0−50% deuterium, this buffer was in H_2O; for 50−100% deuterium, this buffer was in D_2O). The solution was then diluted with an equal volume of H_2O/D_2O solution to yield the appropriate deuterium content. The concentration of ruthenium was found using the MLCT absorbance around 480 nm.

(22) Kreevoy, M. M.; Ostovic, D.; Truhlar, D. G. *J. Phys. Chem.* **1986**, *90*, 3766−3774.
(23) Kim, Y.; Truhlar, D. G.; Kreevoy, M. M. *J. Am. Chem. Soc.* **1991**, *113*, 7837−7847.
(24) Kim, Y.; Kreevoy, M. M. *J. Am. Chem. Soc.* **1992**, *114*, 7116−7123.
(25) Marcus, R. A.; Sutin, N. *Biochim. Biophys. Acta* **1985**, *811*, 265.
(26) Albery, W. J. *Annu. Rev. Phys. Chem.* **1980**, *31*, 227−263.
(27) Takeuchi, K. J.; Thompson, M. S.; Pipes, D. W.; Meyer, T. J. *Inorg. Chem.* **1984**, *23*, 1845−1851.
(28) Lee, I.-S. H.; Jeoung, E. H.; Kreevoy, M. M. *J. Am. Chem. Soc.* **1997**, *119*, 2722−2728.
(29) Maestri, M.; Armaroli, N.; Balzani, V.; Constable, E. C.; Thompson, A. M. *Inorg. Chem.* **1995**, *34*, 2759−2767.
(30) Cook, M. J.; Lewis, A. P.; McAuliffe, G. S. G.; Skarda, V.; Thomson, A. J.; Glasper, J. L.; Robbins, D. J. *J. Chem. Soc., Perkin Trans.* **1984**, 1293−1301.
(31) Welch, T. W.; Neyhart, G. A.; Goll, J. G.; Ciftan, S. A.; Thorp, H. H. *J. Am. Chem. Soc.* **1993**, *115*, 9311−9312.
(32) Farrer, B. T.; Thorp, H. H., to be submitted.
(33) Stultz, L. K.; Binstead, R. A.; Reynolds, M. S.; Meyer, T. J. *J. Am. Chem. Soc.* **1995**, *117*, 2520−2532.
(34) Brereton, R. G. *Analyst* **1995**, *120*, 2313−2336.

Results

Driving Force Effects. Complexes based on $Ru^{II}(tpy)(bpy)OH_2^{2+}$ can undergo loss of an electron coupled to the loss of a proton to yield the hydroxy complex, $Ru^{III}(tpy)(bpy)OH^{2+}$,[27] which can in turn undergo a one-electron, one-proton oxidation to yield the oxo complex $Ru^{IV}(tpy)(bpy)O^{2+}$. The overall oxidation is a two-electron, two-proton transfer:

$$Ru(tpy)(bpy)OH_2^{2+} \leftrightharpoons Ru(tpy)(bpy)OH^{2+} + e^- + H^+ \quad (3)$$

$$Ru(tpy)(bpy)OH^{2+} \leftrightharpoons Ru(tpy)(bpy)O^{2+} + e^- + H^+ \quad (4)$$

The ability of the complex to lose a proton upon oxidation enables electron density from the oxygen to help stabilize higher oxidation states, which is evident in comparing the potentials of the Ru(II/III) couple (eq 3) for $Ru(tpy)(bpy)OH_2^{2+}$ (0.49 V at pH 7)[27] to those of similar complexes without the aqua ligand, such as $Ru(tpy)(bpy)Cl^+$. Since both oxidations require loss of one proton, the oxidation potentials show the same Nernstian pH dependence (−59 mV/pH unit).[27] Thus, both oxidation potentials increase with decreasing pH, but the *difference* in the oxidation potentials remain the same. The pH range, where this statement is valid, is determined by the pK_a's of the different species and is between pH 2 and 10 for $Ru(tpy)(bpy)OH_2^{2+}$. The difference in oxidation potential is important when considering the comproportionation between Ru(II) and Ru(IV) that we describe herein:

$$Ru(tpy)(bpy)OH_2^{2+} + Ru(tpy)(bpy)O^{2+} \leftrightharpoons 2\,Ru(tpy)(bpy)OH^{2+} \quad (5)$$

which requires a transfer of one proton and one electron. This redox reaction is defined by the half reactions shown in eqs 3 and 4. The driving force for eq 5 is, therefore, a function of the potentials for the two half-reactions ($\Delta E_{1/2} = E_{1/2}(III/IV) - E_{1/2}(III/II)$). Kinetically, the forward rate constant is second order overall and first-order in both $RuOH_2^{2+}$ and RuO^{2+}. The rate of the $Ru(bpy)_2(py)O^{2+}$ comproportionation is independent of pH between pH 2 and 10,[16] changing only at pH values where the Ru(III) species is protonated or the Ru(II) species is deprotonated.

As will be discussed below, the kinetics of PCET of RuO^{2+} complexes is very sensitive to the coordination environment about the Ru−O linkage. So, although there are a large number of known polypyridyl oxoruthenium(IV) complexes,[35] many of these differ dramatically in the configuration about the Ru−O linkage. We have shown previously that seemingly subtle changes in the coordination about the Ru center (i.e., from $Ru(tpy)(bpy)O^{2+}$ to $Ru(bpy)_2(py)O^{2+}$ to *cis*-$Ru(bpy)_2(OH_2)O^{2+}$) produce dramatic changes in the selectivity of cleavage of DNA.[36,37] We, therefore, have chosen to investigate the driving force dependence of PCET, using complexes based on $Ru(tpy)(bpy)O^{2+}$, which can be functionalized either on the bpy ligand at the 4 and 4′ positions or on the para position of the central pyridine of the tpy ligand. These sites of substitution do not produce significant perturbation of the steric environment at the Ru−O bond (Figure 1).

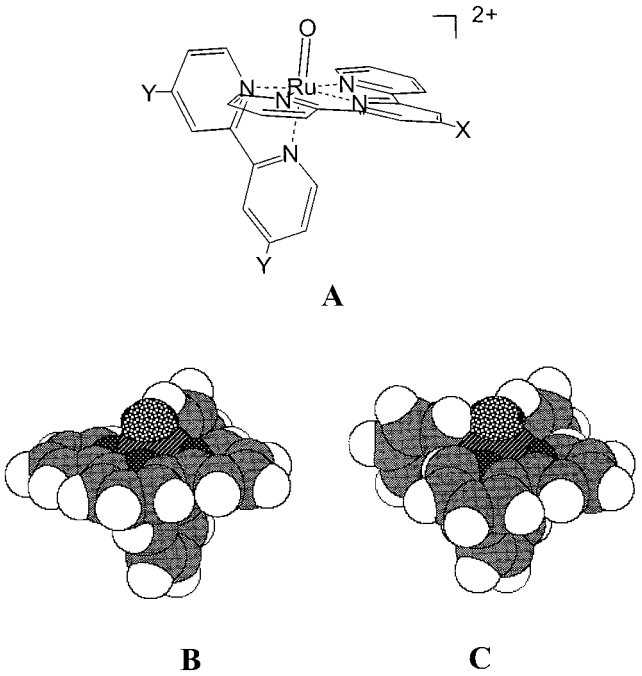

Figure 1. Structures of oxoruthenium(IV) complexes discussed. (A) Schematic drawing of $Ru(tpy)(bpy)O^{2+}$ showing the sites of modification (X, Y), which are far removed from the Ru−O linkage. (B) CPK model of $Ru(tpy)(bpy)O^{2+}$. (C) CPK model of $Ru(bpy)_2(py)O^{2+}$.

Before investigating the isotope dependence of eq 5, we must first determine whether carrying out the reaction in H_2O or D_2O affects the driving force of the reaction. The large isotope effect could be a result of a lower driving force in D_2O compared to H_2O, which would decrease the rate constant, according to Marcus theory, in the normal region where the rate increases with driving force (eq 2). The isotope effect could, therefore, be the result of a normal (<8) kinetic isotope effect coupled with an equilibrium isotope effect, coming from change in driving force.[38] To investigate this matter, exhaustive cyclic voltammetry and square-wave voltammetry studies of all of the compounds were performed in H_2O and D_2O with careful control over pH and pD. For both square-wave voltammetry and cyclic voltammetry, changes in peak potentials upon changing from H_2O to D_2O were observed; however, these changes in peak potentials could always be ascribed to slower kinetics in D_2O rather than a change in the true redox potential.[39−41] In the limit of low sweep rates in either experiment, the potentials in H_2O and D_2O always approached the same limiting values. The $E_{1/2}$(IV/III), $E_{1/2}$(III/II), and $\Delta E_{1/2}$ values for all of the compounds in the series are shown in Table 1.

The series of complexes given in Table 1 were synthesized with the goal of developing a series of isostructural comproportionation reactions with changes in the driving force; as shown in Table 1, changes in $\Delta E_{1/2}$ were in fact obtained across the series. A plot of the $E_{1/2}$ vs driving force (Figure 2) for both the II/III and the III/IV couples shows that the $Ru^{II/III}$ couple is more sensitive to the electron density on the metal than is

(35) Dovietoglou, A.; Adeyemi, S. A.; Meyer, T. J. *Inorg. Chem.* **1996**, *35*, 4120−4127.
(36) Carter, P. J.; Cheng, C.-C.; Thorp, H. H. *Inorg. Chem.* **1996**, *35*, 3348−3354.
(37) Welch, T. W.; Ciftan, S. A.; White, P. S.; Thorp, H. H. *Inorg. Chem.* **1997**, *36*, 4812−4821.
(38) Kreevoy, M. M.; Liang, T.-m.; Chang, K.-C. *J. Am. Chem. Soc.* **1977**, *99*, 5207−5209.
(39) O'Dea, J.; Osteryoung, J.; Lane, T. *J. Phys. Chem.* **1986**, *90*, 2761−2764.
(40) O'Dea, J. J.; Wikiel, K.; Osteryoung, J. *J. Phys. Chem.* **1990**, *94*, 3628−3636.
(41) Bard, A. J.; Faulkner, L. R. *Electrochemical Methods*; John Wiley and Sons: New York, 1980.

Table 1. Redox Potentials of Ru(X-tpy)(Y_2-bpy)O^{2+}

compound	$E_{1/2}$(III/II) (V)[a]	$E_{1/2}$(IV/III) (V)[a]	$\Delta E_{1/2}$ (V)
Ru(EtO-tpy)(bpy)O^{2+}	0.427	0.567	0.139
Ru(tpy)(Me_2-bpy)O^{2+}	0.434	0.574	0.139
Ru(tpy)(bpy)O^{2+}	0.469	0.576	0.107
Ru(Cl-tpy)(bpy)O^{2+}	0.500	0.599	0.099
Ru(tpy)(Cl_2-bpy)O^{2+}	0.507	0.592	0.085

[a] V vs Ag/AgCl from cyclic voltammetry experiments at low scan rates in 50 mM phosphate buffer, pH 7.8.

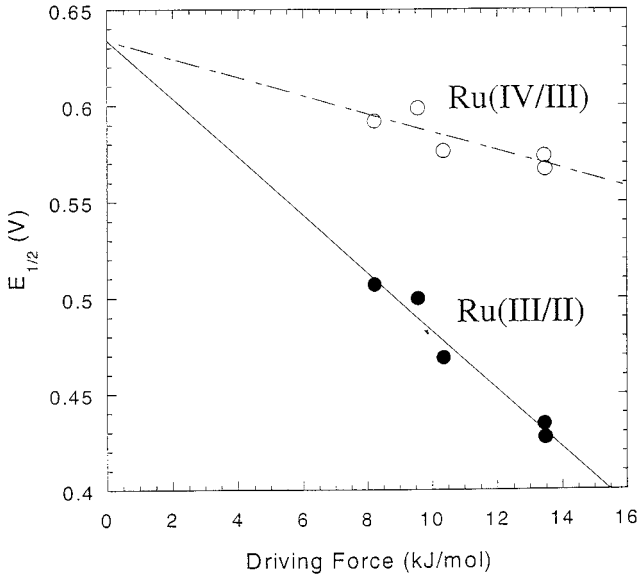

Figure 2. Plot of the redox potentials $E_{1/2}$(IV/III) (○) and $E_{1/2}$(III/II) (●) versus the driving force for comproportionation calculated from $\Delta E_{1/2}$. Potentials are given in V vs Ag/AgCl in 50 mM phosphate buffer (pH 7.8).

the $Ru^{III/IV}$ couple. The slopes are -0.45 ± 0.17 and -1.45 ± 0.17 for the II/III and the III/IV couples, respectively. This observation shows that the +4 oxidation state is more affected by the proton coupling effect than the +3 oxidation state, which is consistent with the correlation noted by Dovletoglu et al.[35] over a series of 22 ruthenium−aqua complexes, spanning a far greater range of potentials than is presented herein (although such a more extensive series of complexes involves drastic changes in coordination and the steric environment about Ru). Presumably, since the overlap of the metal−oxygen π orbitals increases exponentially as the bond length decreases, the change in bond length is a more effective stabilizing force at smaller bond lengths. Therefore, the hydroxy to oxo conversion is more stabilizing than the aqua to hydroxy conversion.

Taken together, the data in Table 1 and Figure 2 demonstrate a series of complexes over which the effects of the driving force and the isotope on the kinetics of eq 5 can be confidently evaluated. The range of driving forces can be extended to about 8 kJ/mol by including the cross reaction of Ru(tpy)(Me_2-bpy)-O^{2+} and Ru(tpy)(Cl_2-bpy)OH_2^{2+}. Although a broader range might be more desirable, the need to preserve the coordination environment about Ru constrains the types of substitutions that can be made.

Comproportionation Kinetics. The kinetics of the comproportionation reaction (eq 5) were followed by stopped-flow spectrophotometry, taking advantage of the known and different absorption spectra of the Ru(II), Ru(III), and Ru(IV) states. The data were fit to a second-order mechanism, using the global fitting program SPECFIT. SPECFIT uses factor analysis by singular value decomposition, which enables the data to be fit without the input of known spectra. A successful fit is then one that not only accounts for the time evolution of the spectra but also predicts the correct absorption spectra for the colored species in the reaction.[33]

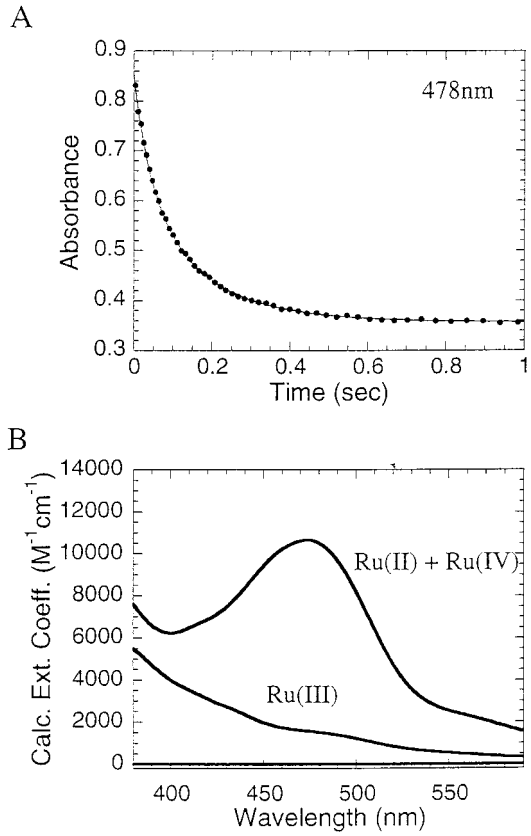

Figure 3. Stopped-flow spectrophotometric data for the comproportionation reaction of 44 μM Ru(tpy)(Me_2-bpy)O^{2+} with 44 μM Ru(tpy)(Me_2-bpy)OD_2^{2+} in 50 mM phosphate buffer (pD = 7.8). Global analysis was performed on the complete data set and fit to the mechanism Ru(tpy)(Me_2-bpy)O^{2+} + Ru(tpy)(Me_2-bpy)OD_2^{2+} ⇌ Ru(tpy)(Me_2-bpy)OD^{2+}. An excellent fit to the time dependence was obtained at all wavelengths (representative data at 478 nm shown in A), and the returned spectra shown in B were in excellent agreement with known spectra taken independently. Note that the analysis returned a blank spectrum and a spectrum that was the sum of Ru(II) + Ru(IV), which was mathematically indistinguishable from returning the two separate spectra.

The comproportionation reaction for Ru($bpy)_2$(py)O^{2+} follows a pseudo-first-order dependence on Ru(IV) in the presence of excess Ru(II).[16] We observed pseudo-first-order kinetics for Ru(tpy)(bpy)O^{2+} with an excess of Ru(tpy)(bpy)OH_2^{2+} and also observed second-order kinetics when the concentrations of Ru(II) and Ru(IV) were equal; the latter condition was more desirable for technical reasons and readily handled by the SPECFIT analysis. Representative kinetics data for the comproportionation of Ru(tpy)(Me_2–bpy)O^{2+} at equal concentrations of Ru(II) and Ru(IV) are shown in Figure 3. A second-order time dependence is observed (Figure 3a), and the calculated spectra returned are in excellent agreement with those for the known Ru(IV), Ru(III), and Ru(II) complexes (Figure 3b). Note that the time dependence was calculated with a starting state that contained a single spectrum for Ru(IV) + Ru(II) and a blank spectrum for the other partner. These two spectra were then evolved to the Ru(III) spectrum, as shown. The use of a sum for one partner in the starting solution is mathematically indistinguishable from using one spectrum for each partner.

Table 2. Rate Constants and Isotope Effects for RuO^{2+} Comproportionation in 50 MM Phosphate Buffer, pH/D 7.8

reaction	driving force (kJ/mol)	$k(H_2O)/10^5\ M^{-1}\ s^{-1}$	$k(D_2O)/10^5\ M^{-1}\ s^{-1}$	$k(H_2O)/k(D_2O)$
$Ru(EtO\text{-}tpy)(bpy)O^{2+} + Ru(EtO\text{-}tpy)(bpy)OH_2^{2+}$	13.5	25.5 ± 3.1	2.40 ± 0.35	10.6 ± 2.0
$Ru(tpy)(Me_2\text{-}bpy)O^{2+} + Ru(tpy)(Me_2\text{-}bpy)OH_2^{2+}$	13.4	29.1 ± 2.4	2.46 ± 0.11	11.8 ± 1.1
$Ru(tpy)(bpy)O^{2+} + Ru(tpy)(bpy)OH_2^{2+}$	10.5	14.9 ± 1.1	1.31 ± 0.12	11.4 ± 1.3
$Ru(Cl\text{-}tpy)(bpy)O^{2+} + Ru(Cl\text{-}tpy)(bpy)OH_2^{2+}$	9.6	11.3 ± 1.2	0.92 ± 0.13	12.3 ± 2.2
$Ru(tpy)(Cl_2\text{-}bpy)O^{2+} + Ru(tpy)(Cl_2\text{-}bpy)OH_2^{2+}$	8.2	5.84 ± 0.24	0.52 ± 0.03	11.2 ± 1.1
$Ru(tpy)(Me_2\text{-}bpy)O^{2+}\ Ru(tpy)(Cl_2\text{-}bpy)OH_2^{2+}$	6.4	4.26 ± 0.25	0.44 ± 0.05	9.8 ± 1.1
$Ru(bpy)_2(py)O^{2+} + Ru(bpy)_2(py)OH_2^{2+}$ [a]	10.4	2.07 ± 0.04	0.135 ± 0.001	16.1 ± 0.4

[a] Data taken from ref 16.

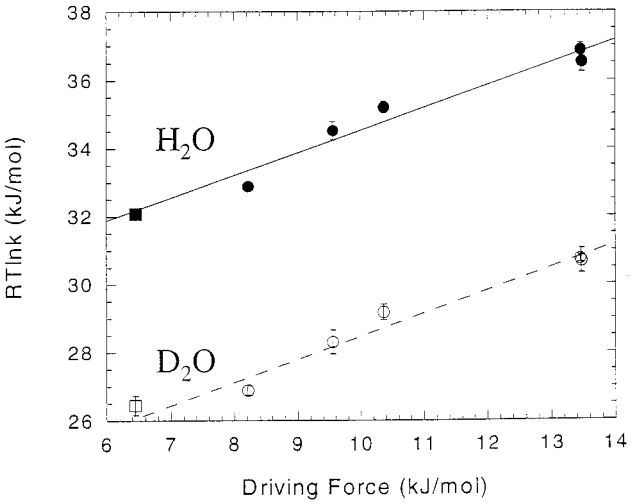

Figure 4. Plot of *RT* ln *k* calculated from data in Table 2 versus the driving force calculated from $\Delta E_{1/2}$ values given in Table 1 for 50 mM phosphate buffer (pH/D 7.8). The data are shown for the comproportionation reactions in H_2O (○), D_2O (○), and the cross reaction in H_2O (■) and D_2O (□). The solid line for the H_2O data gives a slope of 0.66 ± 0.06, and the solid line for D_2O gives a slope of 0.64 ± 0.05. Error bars are for 1 standard deviation.

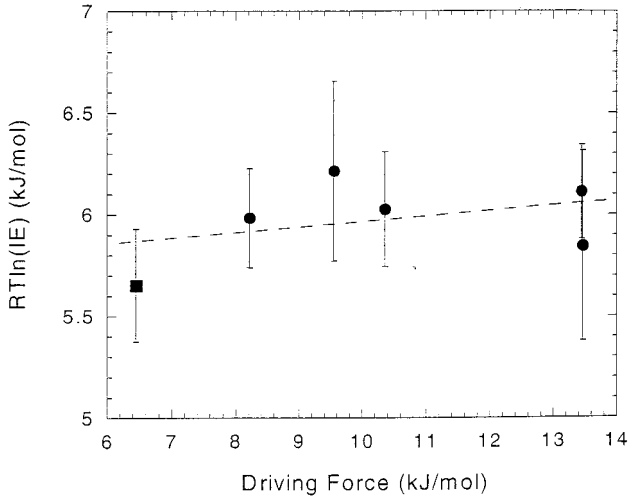

Figure 5. A plot of *RT* ln(IE) where IE is the isotope effect $k(H_2O)/k(D_2O)$ given in Table 2. Results are shown for the comproportionation reactions (●) and the cross reaction (■). Error bars are for 1 standard deviation; note that the *y*-axis has been greatly enlarged compared to Figure 4.

Kinetics data were obtained for the all of the comproportionation reactions and the cross reaction under second-order conditions, as shown in Figure 3. The absorbance spectra predicted from the fitting show good correlation to known absorbance spectra taken independently. The measured second-order rate constants in H_2O and D_2O are shown in Table 2 along with isotope effects. A plot of *RT* ln *k* vs driving force (Marcus plot) is shown in Figure 4. The rates of reaction increase with an increase in driving force as expected from Marcus theory (for electron transfer in the normal region)[25] and the Brønsted relationship (for proton transfer).[26] As shown in eq 2, a slope of 0.5 is predicted by Marcus Theory for proton transfer or electron transfer. For the comproportionation reactions in Figure 4, the slopes of 0.66 ± 0.06 and 0.64 ± 0.05 are found for H_2O and D_2O reactions, respectively. Given the relatively narrow range of available driving forces, we consider these values to be in reasonable agreement with the Marcus prediction of $^1/_2$.

The slopes for the driving force dependence in both H_2O and D_2O are the same within experimental error. Thus, there is no detectable dependence of the isotope effect on the driving force, as predicted for eq 2 in the linear ($\Delta G°/2$) region. This point is emphasized by a plot of the $\ln(k_H/k_D)$ vs driving force (Figure 5); the slope of the least-squares line in this plot is -0.017 ± 0.031. To ensure that there was only one proton in the reaction, the rate constant was measured as a function of D_2O composition and found to vary linearly (Figure 6). A similar proton inventory was observed for the $Ru(bpy)_2(py)O^{2+}$ reaction.[16]

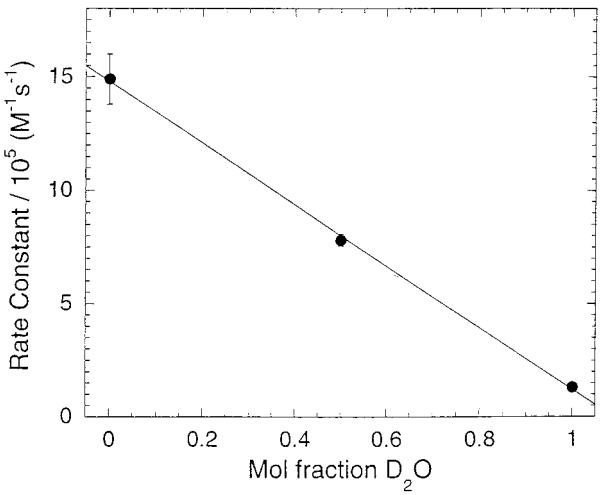

Figure 6. Proton inventory plot for the comproportionation between $Ru(tpy)(bpy)O^{2+}$ and $Ru(tpy)(bpy)OH_2^{2+}$ in 50 mM sodium phosphate buffer (pH = pD = 7.8).

Discussion

The results described herein show that the comproportionation reaction (eq 5) of $Ru(tpy)(bpy)O^{2+}$ involves only a single proton and obeys the predicted second-order kinetics. The series of electronically differentiated complexes provides a range of driving forces of ~8 kJ/mol over which the reaction rates can be investigated. The large difference between the isotope effects for $Ru(tpy)(bpy)O^{2+}$ and $Ru(bpy)_2(py)O^{2+}$ shows that the chosen series of complexes must be one that includes no steric perturbations proximal to the Ru−O linkage, which is well

satisfied by the series chosen herein. (Note that the driving force for the $Ru(bpy)_2(py)O^{2+}$ reaction is within the range encompassed by complexes used herein.) Across this driving force range, the rate constant increases with increasing driving force, as expected for Marcus electron (or proton) transfer in the normal region. Further, the slope of the plots for both H_2O and D_2O is only slightly higher than the value of 0.5 predicted from the Marcus equation.

The effect of sterics upon proton-coupled electron transfer can be understood by comparing the results herein to the data taken previously by Binstead and Meyer[15,16] for a similar but more sterically crowded oxo complex, $Ru(bpy)_2(py)O^{2+}$ (Figure 1). Data from the previous study indicated that the isotope effect was pH independent from pH 4 to 10, the comproportionation rate constant varied linearly with D_2O content, and the isotope effect was 16.1. This isotope effect is significantly higher than the one found here in the $Ru(tpy)(bpy)O^{2+}$ system. Since the driving force for the $Ru(bpy)_2(py)O^{2+}$ system is slightly different, we must calculate the isotope effect for the same driving force for the $Ru(tpy)(bpy)O^{2+}$ system from the plot in Figure 4, which gives an isotope effect of 11.5, significantly lower than the 16.1 value for the $Ru(bpy)_2(py)O^{2+}$ system. The absolute magnitude of the comproportionation rate constant for the $Ru(bpy)_2(py)O^{2+}$ complex is also much slower ($2.18 \pm 0.032 \times 10^5\ M^{-1}\ s^{-1}$) than that for the corresponding $Ru(tpy)(bpy)O^{2+}$ complex (calculated to be $12.7 \times 10^5\ M^{-1}\ s^{-1}$ after correction for a change in ionic strength between the results herein and those in ref 16).

The increase in isotope effect and decrease in rate suggest that the sterics of the pyridine ligand have a significant effect on the mechanism of comproportionation. Meyer has suggested that the tunneling of the proton from one oxygen to the other while an electron tunnels from one ruthenium to the other is the cause of the large isotope effect.[16] This idea is supported by the present data. As evident in Figure 1, $Ru(bpy)_2(py)O^{2+}$ is more sterically crowded than the $Ru(tpy)(bpy)O^{2+}$ complex because there are two pyridines parallel to the Ru−O linkage in $Ru(bpy)_2(py)O^{2+}$ and only one in $Ru(tpy)(bpy)O^{2+}$. Thus, the rate for $Ru(bpy)_2(py)O^{2+}$ is expected to be slower according to both the classical and tunneling theories. Thus, the significant increase in the isotope effect over the classical limit can be explained by a significant tunneling distance for the proton, which is larger in $Ru(bpy)_2(py)O^{2+}$ than in $Ru(tpy)(bpy)O^{2+}$.

Acknowledgment. We thank Professor T. J. Meyer and Dr. R. A. Binstead for numerous helpful discussions. This research was supported by the National Science Foundation.

IC9902323